Journal of Materials Chemistry C

ROYAL SOCIETY OF CHEMISTRY

PAPER

View Article Online
View Journal | View Issue

Cite this: J. Mater. Chem. C, 2026, 14, 205

On the photothermal behaviour of naphthalene diimide aggregates in water

Ziyao Xu,[a] James Doutch,[b] Najet Mahmoudi,[b] Stephen Sproules[a] and Emily R. Draper *[a]

Photothermal effects, driven by the conversion of light into heat, offer versatile applications in fields such as photothermal therapy, energy conversion, and pollution degradation. Naphthalene diimide (NDI) molecules exhibit diverse properties with applications spanning optoelectronics, materials science, and nanomedicine. In this study, we synthesize various amino acid-functionalized naphthalene diimides, which, after irradiation with light in both gel and solution forms, produce radical anions, which enables their photothermal properties. Our findings demonstrate the influence of pH on photothermal performance. Furthermore, we demonstrate that the incorporation of polyvinyl alcohol (PVA) increases the viscosity of the solutions and reduces oxidation. To further investigate how pH affects the aggregated structures, we use small-angle neutron scattering (SANS). In addition, *in situ* SANS measurements were conducted to monitor the aggregation changes during irradiation to advance our understanding of NDIs' potential as photothermal materials in potential energy-related applications.

Received 18th August 2025,
Accepted 14th October 2025

DOI: 10.1039/d5tc03120f

rsc.li/materials-c

Introduction

Photothermal effects, fuelled by the conversion of light energy into heat, are gaining prominence. Light sources that are necessary for inducing the photothermal effect can use sunlight or internal lighting, which are readily available, inexhaustible, renewable, and sustainable, making them increasingly popular. Consequently, photothermal technology finds diverse applications across various fields, owing to its accessibility and versatility. In biomedicine, photothermal materials enable targeted cancer therapy through localized heating of tumor cells.[1–5] In energy conversion, they capture sunlight for power generation.[6–9] They can also facilitate high-resolution imaging and sensing in photonic devices.[10] Traditional photothermal materials, such as gold and silver nanoparticles, as well as carbon-based materials like graphene and transition metal chalcogenides, exhibit strong photothermal properties but often suffer from limited biocompatibility, higher cost, potential environmental concerns, and less flexibility compared to organic materials. While these inorganic materials show promise in various applications, including photothermal therapy and energy conversion, the advantages of organic materials, such as better biocompatibility, lower cost, reduced environmental impact, and improved flexibility, make them increasingly attractive for photothermal applications in biomedical, environmental, and energy fields. Polydopamine (PDA),[11] photoresponsive liquid crystal elastomers, and polymer networks[12] are in many cases particularly intriguing because of their physical properties, low cytotoxicity, biodegradability, *etc.* Near-infrared (NIR)-absorbing organic nanoparticles (ONPs) are emerging candidates for photothermal therapy. For example, Zhang *et al.* synthesised a new porphyrin–diketopyrrolopyrrole (Por–DPP) which exhibited photothermal effects suitable for photothermal therapy under 808 nm laser irradiation.[13] Some small organic molecules have also been studied, like in the work of Zhu *et al.*, who designed and synthesised a small molecule where perylene diimide was used as an electron acceptor while triphenylamine was used as an electron donor. These two materials were conjugated through a triple bond which enhanced the π conjugation of the system, leading to a red shift in the absorption spectrum.[14] Other organic dyes, such as cyanine dyes and porphyrins, have strong absorption in the visible and near-infrared regions, allowing them to absorb light and convert it into heat, making them suitable for photothermal applications.

Naphthalene diimides (NDIs) have been shown as a fascinating class of molecules due to their electronic properties, large electron-deficient aromatic cores, and tendency to self-assemble into functional structures, leading to a wide variety of applications ranging from biomedicine to electronics. NDIs also possess high electron affinity, are able to form a radical anion and dianion upon reduction[15,16] (Fig. 1(a)), have good charge carrier mobility, and excellent thermal and oxidative stability, making them promising candidates for organic electronics applications, photovoltaic[17] devices, and flexible displays.[18] There are examples

[a] School of Chemistry, University of Glasgow, Glasgow, G12 8QQ, UK. E-mail: Emily.Draper@glasgow.ac.uk
[b] ISIS Neutron and Muon Source, Rutherford Appleton Laboratory, Oxfordshire, OX11 0QX, UK

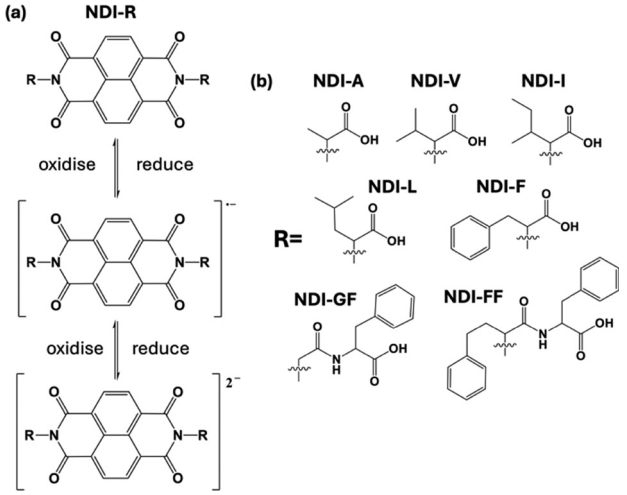

Fig. 1 The general chemical structure of the naphthalene diimide used in this study: (a) redox process to achieve the radical anion and dianion and (b) R groups used in the imide position, based on amino acids and dipeptides.

from the literature where NDI scaffolds have shown strong NIR absorption by the use of dendritic and anionic donors[19,20] and therefore are good candidates for photothermal behaviour. Within our own research, we showed that a gelled perylene bisimide material exhibited notable photothermal effects, making it a potential candidate for application in the field of photothermal materials. Compared to these perylene materials, we observed that naphthalene diimide (NDI) molecules possess greater solubility (making them easier to process into films) and NIR absorption characteristics as well as the ability to change their aggregation based on pH and therefore their electronic and optical behaviour.[21] We therefore investigate here whether these different aggregates would lead to photothermal behaviour in these materials. Building on findings from our previous studies on NDI materials,[22] we focus here on 7 NDI molecules functionalised at the imide position with various amino acids and dipeptides, examining how changes in pH and concentration and consequently solubility affect their absorption and photothermal properties (Fig. 1b). Small-angle neutron scattering (SANS) provides detailed insights into the internal aggregation structures and the influence of pH on these assemblies. *In situ* irradiation SANS of the materials further helps us understand the relationship between molecular aggregation and the formation of radical anions using light as well as stability and reversibility of our systems. Through this systematic exploration, we aim to gain valuable insights into the potential of NDI-based materials for photothermal applications.

Results and discussion

In order to investigate the photothermal effect, we must first generate the radical anion (Fig. 2). This can be achieved by photoreduction with UV light and easily seen both by eye and by using UV-vis absorption spectroscopy. Using this method, we can assess the amount of radical and compare our materials.

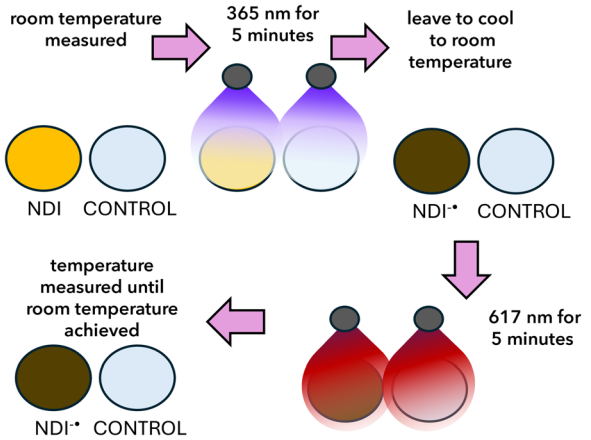

Fig. 2 Cartoon showing how the photothermal measurements were carried out.

To generate the radical anion, we used 365 nm irradiation for 5 minutes (Fig. 3a). The samples were then allowed to cool to room temperature before using a visible wavelength of light where the radical anion absorbs; here we use 617 nm irradiation for 5 minutes. The resulting change in temperature was then measured using a photothermal camera. Control experiments were conducted using water and NDIs that had not been irradiated with UV light and the radical was not generated (Fig. S16, SI). Water was collected each time, and a set of experiments were run to mitigate the difference in room temperature on different days. These controls showed that the NDI radical

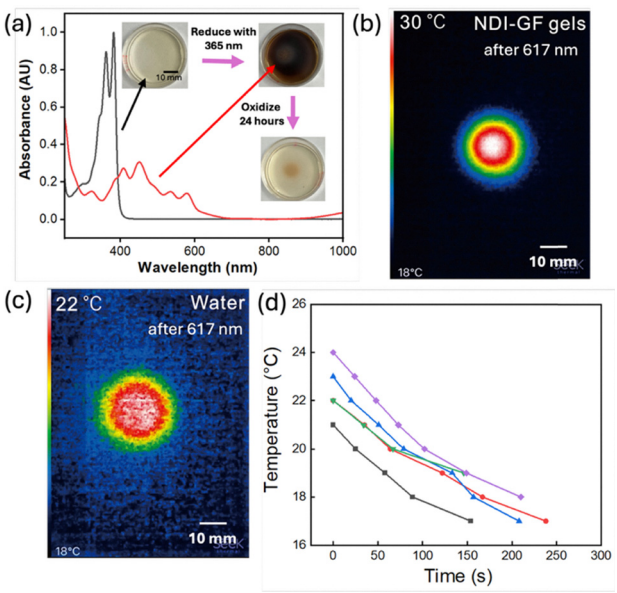

Fig. 3 (a) UV-vis absorption profiles of the neutral species (black) and reduced species (red) of NDI-GF gels. Inset photographs of the neutral, reduced and oxidised solutions. Photothermal images after irradiation with 617 nm of (b) the NDI-GF gel and (c) water. (d) Change in temperature over time after irradiation with 617 nm of NDI-GF solutions at pH 8 at concentrations of 1 (black), 2 (red), 5 (blue), 10 (green) and 20 mg mL^{-1} (purple).

was needed to produce the photothermal effect. All the photothermal measurements were conducted in this way.

We have previously shown that NDI-GF can form gels at low pH and various aggregated structures at different pHs. We have thoroughly characterised these materials using SANS, UV-vis absorption spectroscopy and electrochemistry in previous studies investigating electrochromic and photochromic behaviour. We therefore started our investigation using NDI-GF.[23] NDI-GF hydrogels were prepared at a concentration of 5 mg mL^{-1} using a pH-switch method, in which 5 mg mL^{-1} glucono-δ-lactone (GdL) was added to induce gelation, resulting in a gel at around pH 3.[23] We then also investigated any concentration effects in the NDIs (1, 2, 5, 10 and 20 mg mL^{-1}). Our results showed that both the gel and solutions exhibited photothermal effects. Thermal images (Fig. 3b) demonstrated a significant difference in heating between equal volumes of the NDI-GF gel and water. While both samples started at the same background temperature (18 °C), the final temperature of the NDI-GF gel reached 30 °C, compared to only 22 °C for water (Fig. 3c). This confirms that the observed photothermal effect is due to the presence of NDI-GF.

Next, the influence of the concentration of NDI-GF solutions was investigated at pH 9. As shown in Fig. 3d, the photothermal measurements showed that a concentration of 20 mg mL^{-1} had the biggest change in temperature which increased by 8 °C. This difference was expected due to the presence of more material and therefore more radical anions. However, the relationship between the concentration and magnitude of photothermal effects does not appear to be linear; this could be due to a complication from diffusion and different structures and amounts of structures being present influencing this (Fig. S17). Under the same conditions, the cooling curve of a 5 mg mL^{-1} solution is close to that of a 10 mg mL^{-1} solution. We then chose 5 mg mL^{-1} for the rest of the pH and other NDI investigations, as it would be the most cost-effective with similar photothermal efficiency to the higher concentrations.

From our previous studies, we saw that differently appended NDIs formed various morphologies at different pHs, which then had different behaviours such as the colour, cyclability and stability of the reduced state. We therefore further studied 7 different amino-acid appended NDIs (as shown in Fig. 1), to investigate whether they would also differ in their photothermal behaviour. We carried out the same experiments as discussed above. Each of the synthesized materials was then dispersed at a concentration of 5 mg mL^{-1} in water at pH 8. As shown in Fig. 3 and 4, NDI-GF, NDI-A, NDI-I, NDI-L, NDI-F, and NDI-V solutions formed radical anions after irradiating with 365 nm light which can be detected by the growing peaks in the range of 490 nm to 650 nm. We also see that each of these materials forms some dianions as well (a decrease at 400 nm and changes in the intensity of peaks from 490–650 nm). The aggregation of the neutral species is similar, with two defined peaks at 370–390 nm and two less defined shoulders at 360 and 350 nm. There are differences in the ratio of peaks at 370 : 390, highlighting subtle differences in the packing of the structures in solution. The most different

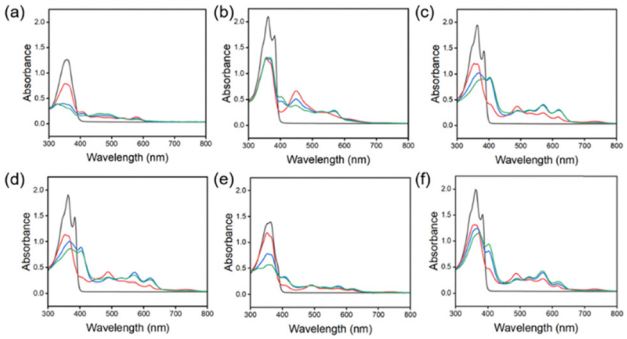

Fig. 4 UV-vis absorption spectra of (a) NDI-GF, (b) NDI-A, (c) NDI-I, (d) NDI-L, (e) NDI-F, and (f) NDI-V before (black data) and after irradiating with 365 nm light for 10 s (red), 60 s (blue), and 300 s (green).

material is NDI-FF (Fig. S18). Before irradiation, NDI-FF has a λ_{max} which is blue shifted compared to other materials and already seems to contain only the dianion. This could indicate that the material is electronically different from the other NDIs in this study and is more light sensitive and so exists already as the dianion. After irradiation, there is a small change in the amount of radical anion, but this is very small; therefore, we were not able to use this material for the photothermal experiments, as there was no change in temperature. NDI-GF and NDI-F show different behaviour from the rest of the NDIs upon irradiation. The other materials show a mixture of the neutral species, the radical anion and dianion, whereas NDI-GF and NDI-F have a majority of the radical anion and dianion, with little neutral species remaining. These differences in radical amount are unlikely due to molecular stacking at this length scale, as it is very similar to the other materials shown, so this difference could be due to the larger aggregates formed being able to stabilise the radical anion/dianion formed. It should also be noted that NDI-GF is the only material investigated that could form a gel, again indicating that the larger scale structures are different.

To further investigate the radical anion/dianion presence, we collected the UV-vis absorption spectra for each of the materials at different pHs (Fig. S19–S72). The data showed that for most of the materials, a radical is formed initially and upon further irradiation, a dianion is also formed. As there seems to be poorly resolved mixtures of species, we also chemically reduced NDI-I using sodium dithionate (Fig. S73) to produce the radical anion and dianionic species. These data further confirm a mixture of the species.

We note that we are unable to carry out this characterisation for the samples used for the photothermal studies. This is due to oxidation during the transfer of the sample into the cuvettes for the measurements. So, in order to further confirm the presence of the radical anion in solution, we conducted EPR spectroscopy on each of the solutions (Fig. S74). All samples, apart from NDI-FF, showed a signal, confirming the presence of the radical species in these samples. The pattern of hyperfine splitting is a result of coupling to the protons and nitrogen nuclei in the NDI and attached amino acid. The asymmetric substitution in NDI-GF produces additional splitting given the

inequivalent chemical environments of the coupled nuclei. This sample also shows differences in UV-vis absorption spectroscopy with the NIR absorption. There are differences between all the samples, with the signal from NDI-A being much weaker (and less resolved) than those of NDI-F and NDI-GF.

As the solution pH has been shown to result in different aggregated states being present in the NDIs, we then looked at the behaviour at different pHs.[21,24] Titration was used to determine the "apparent" pK_a values (Fig. S75–S80) and to assess any correlations with observable changes. Table S1 presents the two apparent pK_a values of NDI solutions according to the pK_a titration curve. These two pK_a values correspond to the two different COOH groups on the NDIs. Rather than the chemically identical COOH groups having different pK_a values, this actually corresponds to a change in solubility and therefore the aggregated state of the material.[21,24] Solutions of NDI-GF, NDI-A, NDI-I, NDI-L, NDI-F, and NDI-V (5 mg mL^{-1}) were prepared separately at pH values ranging from 2 to 10. Notably, we observed that the appearance of the NDI solutions (Fig. 5 and Fig. S81) changed at pH values close to their respective pK_a values.

Below pH 5, the materials precipitated out of solution due to loss of solubility. Above pH 7, the solutions became deeper in colour, and then at pH 10, the materials were less coloured. This all again agrees with the apparent pK_a values of the materials, demonstrating that different aggregated materials are present. In addition, NDI-GF has a different colour to the rest of the materials and looks darker brown compared to the yellow colour of the other NDIs. We observe, upon lowering the pH of the materials in solution, a red shift in the λ_{max}, suggesting that H-type aggregation occurs which we have observed before with these types of materials.[21] The results confirmed that pH directly affects the formation of radical anions during irradiation, with different amounts of radical formed and some shifting in peak positions depending on pH. However, NDI-I and NDI-V appear to be the least affected by pH, with the radical species seeming unchanged by the different pHs. NDI-I and NDI-V have similar branched side chains, and again this could be something to do with the packing of the molecules.

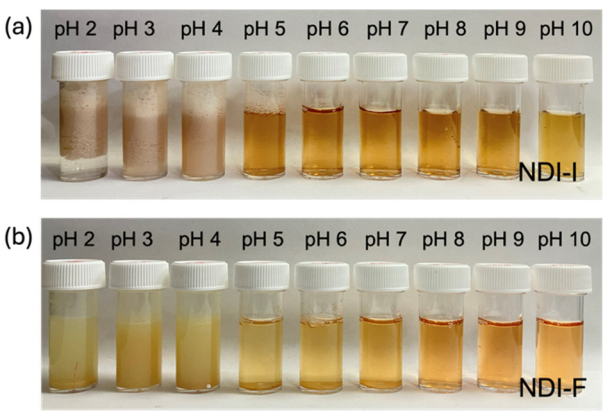

Fig. 5 Photographs of (a) NDI-I and (b) NDI-F at 5 mg mL^{-1} and different pHs.

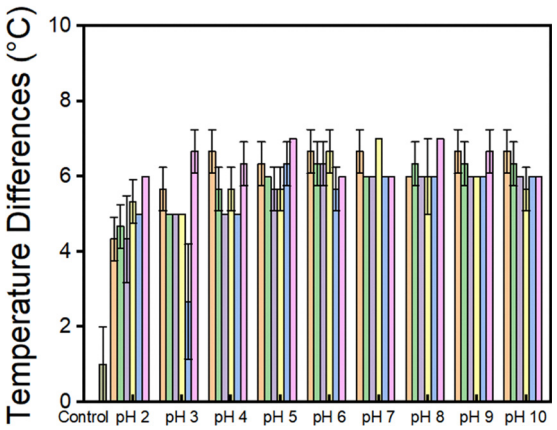

Fig. 6 Temperature differences of NDI solutions at pHs 2–10 from the photothermal experiment. NDI-A (orange), NDI-V (green), NDI-L (purple), NDI-I (yellow), NDI-F (blue) and NDI-GF (pink). Error bars are calculated from the standard deviation of three repeated measurements.

The photothermal effect of all the NDIs at the different pHs was then investigated. As shown in Fig. 6, in general lower pH values generally corresponded to smaller temperature changes across all NDI samples, suggesting that greater molecular aggregation results in a reduced photothermal effect. It appeared that, for most of the NDIs, as the material is closer to its 2nd pK_a, the performance improves. Above pH 7, there does not seem to be much change in the performance of the materials. NDI-GF again is different, as it exhibits better performance at lower pHs. This could be due to its ability to gel rather than precipitate. We saw that the bulk precipitate showed very little colour change after prolonged irradiation with 365 nm light (Fig. S82) which was different compared to the materials that were soluble. Among the tested solutions, in general NDI-I exhibited the highest ability to convert light energy into heat, as indicated by its final temperature difference at pH 7. It also showed the biggest pH dependence in its performance, which is contrary to what is seen by UV-vis absorption spectroscopy. In contrast, the temperature differences of NDI-L, NDI-F, and NDI-V showed minimal correlation with pH. Notably, NDI-F displayed the least radical ion from absorption spectroscopy, and its final temperature difference was also the lowest. We have seen a similar interesting pH dependence which does not seem to correlate with the chemical structure and amount of radical anion when using NDIs for chromic applications.[21] It was hypothesised that the low viscosity of the materials could impact the heat diffusion and performance of the materials; therefore, we included a thickening agent into the systems. We chose PVA at 5 wt%. Indeed, the addition of polymer increases the viscosity of the solution (Fig. S83 and S84). Next, the photothermal properties were measured using the same setup and under identical LED output power for all samples. Since low pH can lead to precipitation of NDI, measurements were only conducted at pH 5, 8, and 10. As shown in Fig. S85, the temperature rise of NDI-PVA solutions is 1 or 2 °C higher than that of NDI solutions without PVA. This enhancement is likely due to the increased

viscosity, which suppresses heat dissipation or reduces oxidation of the radical anion. We therefore used PVA in the remainder of the investigations.

In order to further investigate the differences in the systems, we used SANS to characterise the morphology of the aggregated systems. We use here 10 mg mL^{-1} of NDI to achieve high enough scattering intensity data. We saw in an earlier study that 5 and 10 mg mL^{-1} showed similar performance, and we show by UV-vis absorption spectroscopy that upon dilution, the structures do not change, and the amount of radical present is proportional to this dilution of structures rather than a change in structure (Fig. S17). These concentration-dependent spectra show a gradual, monotonic increase in absorbance without a sigmoidal transition, which is more consistent with an isodesmic assembly process. Not only were we able to characterise the morphology of the systems at different pHs, but we were also able to determine if these aggregates changed upon the irradiation of the systems with UV or red light. This would give us an indication of the stability and reversibility of the materials with respect to the photothermal effect.

Specifically for SANS, we compared PVA/NDI-I and PVA/NDI-F systems, with pure PVA used as a blank control. This was due to NDI-F showing the poorest response and NDI-I showing the best, and most pH dependent behaviour. The data fitting and parameters are presented in Fig. S86 and Table S2. Pure PVA was best fitted with an elliptical cylinder model combined with a power law, showing a minor radius of approximately 10.71 Å and an axial ratio of around 3.75, indicating a notably elliptical shape with an estimated length of 162.5 Å. In contrast, all the PVA/NDI systems were well-fitted with a cylindrical model combined with a power law. This suggests that the incorporation of NDI transforms the structures in solution, with the two materials possibly interacting with each other.

To study the influence of pH on aggregation, pH levels of 5, 8, and 10 were selected. As shown in Fig. 7 and detailed in Tables S3 and S4, the pH did not alter the morphology (*i.e.*, the fitted model remained cylindrical), but it did slightly affect the dimensions of the cylindrical aggregates. Specifically, both the radius and length increased modestly with rising pH, indicating that pH variations from 5 to 10 have a limited impact on the photothermal performance. Interestingly, PVA/NDI-F exhibited a different trend: at pH 8, the structure showed the largest radius of 21.12 Å but the shortest length of 94.78 Å, while the structures at pH 5 and 10 appeared similar. Notably, PVA/NDI-F also demonstrated the best photothermal performance at pH 8, which may correlate with these changes in aggregate structure.

Next, we performed *in situ* irradiation whilst collecting the SANS data using the wavelengths of light used in the photothermal experiments. We know that temperature can affect the aggregation of self-assembled materials[24] and that the presence of radicals could also affect the aggregation. To explore this, we looked at *in situ* oxidation cycles after 365 nm irradiation and *in situ* photothermal treatment with 617 nm light, comparing with offline irradiation and oxidation cycles using 365 nm light. Compared to the non-irradiated sample (PVA/NDI-I at pH 5), the samples exposed to 365 nm light, both during and after

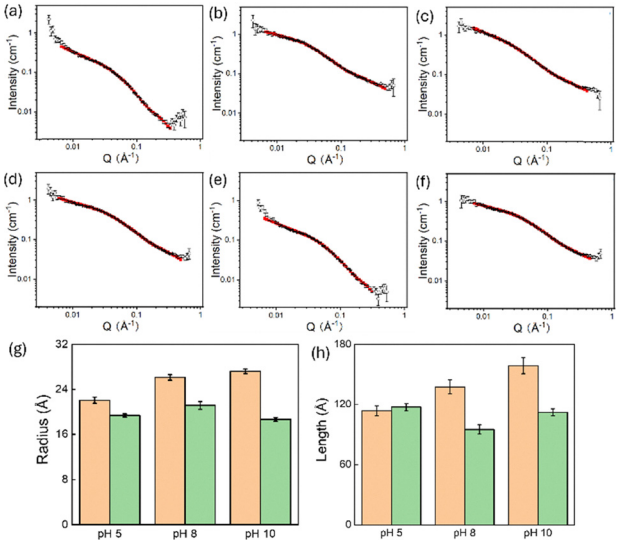

Fig. 7 SANS data and fits from PVA/NDI-I at pH 5 (a), pH 8 (b), and pH 10 (c). SANS data and fit for PVA/NDI-F at pH 5 (d), pH 8 (e), and pH 10 (f). For (a)–(f), the data are shown as open circles and the fits to the data as red points. (g) Radius and (h) length of structures from SANS at pH 5, 8 and 10 for NDI-I/PVA (orange) and NDI-F/PVA (green).

irradiation (Fig. S87 and Table S5), maintain a similar radius (22.8 Å before, 22.0 Å during, and 21.3 Å after irradiation), but show an increase in length (113 Å before, 134.9 Å during, and 134.5 Å after irradiation). In contrast, during irradiation with 617 nm light, the radius increases while the length decreases, likely due to heat generation by radicals, causing a slight structural contraction. After irradiation with 617 nm light ceases, the photothermal effect dissipates, and the structure gradually returns to its original length and radius. For PVA/NDI at pH 8, the behaviour differs notably (see Fig. S88 and Table S6). During irradiation with 365 nm light, the radius remains unchanged (26.1 Å before, during, and after irradiation), while the structure elongates temporarily (137.5 Å before and 141.7 Å during) and then returns close to its original length after irradiation ends (136.6 Å). Under 617 nm irradiation, however, the radius slightly decreases, and the length becomes shorter after irradiation. These observations suggest that PVA/NDI may exhibit different aggregation behaviours depending on the pH and that its response to irradiation varies accordingly.

In situ oxidation experiments were conducted on PVA/NDI-I at pH 8, with approximately 1-hour intervals between each measurement to allow for oxidation in air (Fig. S89 and Table S7). Following 365 nm irradiation, the radius decreased from 26 Å to around 23 Å and remained relatively constant thereafter. The structural length showed a more pronounced decrease, dropping from 136 Å to 119 Å immediately after irradiation (oxidation 1), and then remained stable at this level in subsequent measurements. We propose that the presence of the PVA polymer slows the oxidation process and contributes to structural stabilization, making further oxidation more difficult beyond this point.

After irradiation with 365 nm light, *in situ* irradiation of PVA/NDI-I with 617 nm light was conducted to generate heat *via* radical anion formation (see Fig. S90, S91 and Tables S8, S9).

During this process, the radius decreased slightly from 26 Å to 24 Å and remained stable throughout. The cylindrical length gradually decreased from 136 Å to 132 Å in the first cycle and then further to 124 Å, stabilizing at this value during subsequent cycles. These results indicate that *in situ* irradiation with 617 nm light does not significantly alter the structure beyond the initial change in length and radius.

Offline irradiation and oxidation experiments were conducted on PVA/NDI-I, as the system demonstrated the ability to generate radical anions repeatedly and without limitation (see Fig. S92 and Table S10). Compared to the original, non-irradiated sample, the structure after the second cycle of irradiation and oxidation showed significant changes. For PVA/NDI-I at pH 5, both the radius and length increased after two cycles. In contrast, at pH 8, the radius remained relatively constant while the length decreased from 137 Å to 128 Å. At pH 10, the length decreased even more substantially, from 158 Å to 136 Å. These observations suggest that pH plays a crucial role in determining the structural response to irradiation, with lower pH (greater protonation) promoting stronger aggregation after irradiation.

When analysing a single sample over multiple cycles (see Fig. S93 and Table S11), different trends emerged, with structural changes being more pronounced. For the sample at pH 8, the length decreased from 137 Å to 128 Å after two cycles, and despite allowing one hour for oxidation, the sample may not have been fully re-oxidized. This suggests that with each cycle, the concentration of radical anions could accumulate. By the fifth cycle, the length had decreased markedly to 90 Å, indicating that repeated generation of radical anions may lead to substantial structural contraction in PVA/NDI-I at pH 8.

For *in situ* irradiation of PVA/NDI-F at pH 8 (see Fig. S94 and Table S12), a slight decrease in both radius and length was observed after 365 nm irradiation. When 617 nm *in situ* irradiation was applied following 365 nm irradiation, the length increased during irradiation but returned to its original value afterward, while the radius showed only a minimal decrease. In the case of offline irradiation and oxidation cycles for PVA/NDI-F at pH 8 (Fig. S95 and Table S13), a significant increase in structural length was observed after the second cycle, with the radius remaining constant. After five cycles, the length appeared to reach a plateau, remaining similar to that observed after the second cycle. From all these observations, we can see the morphology of the fibre-like structures changing in radius and length with no observable disaggregation occurring, which is also seen with the spectrophotometry results above. This suggests that the structural changes stabilized after multiple cycles and that radical anion generation *via* irradiation can occur repeatedly. All these data are promising as the samples show stability and/or reversibility of the structures, indicating longevity in the structures.

Conclusions

In summary, we have developed NDI-based photothermal materials and demonstrated that radical anions can be generated upon irradiation with 365 nm light; these reduced NDI species then demonstrate the photothermal effect upon irradiation with 617 nm. The materials were able to increase the temperature by 8 °C compared to their environment. This change in temperature was dependent on both pH and the R group present in the imide position of the NDI. All the materials show the best photothermal behaviour above pH 5. This pH-dependent behaviour is determined by the pK_a of the different materials which in turn influences the morphology of the self-assembled NDIs. Below the second pK_a, the materials tend to precipitate from solution. However, the materials were less affected by concentration but tended to have a slightly larger change in temperature at higher concentrations. This is probably due to more radical anions being present, but it was not significant. Using SANS, we showed that cylindrical structures formed in solution in the presence of PVA and that at various pH values and upon irradiation and oxidation, their radius and/or length changed but did generally return to the original dimensions. This implies that the NDIs are stable and could withstand multiple photothermal cycles, and the changes are more likely due to the presence of the radical anion rather than dissembling due to the change in temperature. These results open up the possibility of using the self-assembly of NDI materials in photothermal applications, with the temperature change being tuned by pH and the NDI group for specific applications.

Author contributions

Ziyao Xu: conceptualization, methodology, investigation, data curation, and writing – original draft. James Doutch and Najet Mahmoudi: helping with SANS data collection and analysis. Stephen Sproules: investigation, data curation, and writing – reviewing and editing. Emily R. Draper: conceptualization, supervision, writing – reviewing & editing, and funding acquisition.

Conflicts of interest

There are no conflicts to declare

Data availability

The SANS data were collected under RB numbers RB2420134 and RB2510438 at the ISIS Neutron and Muon Source. The datasets are available at DOI: **https://doi.org/10.5286/ISIS.E.RB2420134-1** and DOI: **https://doi.org/10.5286/ISIS.E.RB2510438-1**.

The data supporting this article have been included as part of the supplementary information (SI). Supplementary information: experimental, synthesis procedures, protocols and supplementary figures. See DOI: **https://doi.org/10.1039/d5tc03120f**.

Acknowledgements

ERD thanks the UKRI (MR/V021087/1) for funding. ZX gratefully acknowledges financial support from the China

Scholarship Council (CSC) and the University of Glasgow through their joint PhD programme. The authors thank the ISIS Neutron and Muon Source (UK) for provision of beamtime for SANS measurements and Maksim Schastny for the design of the LED irradiation cell and help with beamtime, and Dr Alex Loch, Dr. Rebecca Ginesi, and Dr. Nicholas Murray for assistance during the beamtime experiments. This work benefitted from SasView software, originally developed by the DANSE project under NSF award DMR-0520547.

Notes and references

1 R. Chang, Q. Zou, L. Zhao, Y. Liu, R. Xing and X. Yan, *Adv. Mater.*, 2022, **34**, e2200139.
2 Y. Xiong, Y. Rao, J. Hu, Z. Luo and C. Chen, *Adv. Mater.*, 2023, e2305140, DOI: **10.1002/adma.202305140**.
3 X. Zhen, C. Xie, Y. Jiang, X. Ai, B. Xing and K. Pu, *Nano Lett.*, 2018, **18**, 1498–1505.
4 H. Sun, Q. Zhang, J. Li, S. Peng, X. Wang and R. Cai, *Nano Today*, 2021, **37**, 101073.
5 X. He, Y. Hao, B. Chu, Y. Yang, A. Sun, K. Shi, C. Yang, K. Zhou, Y. Qu, H. Li and Z. Qian, *Nano Today*, 2021, **39**, 101210.
6 L. Zeng, D. Deng, L. Zhu, Z. Zhang, X. Gu, H. Wang and Y. Jiang, *Nano Energy*, 2024, **125**, 109531.
7 Y. D. Zhao, W. Jiang, S. Zhuo, B. Wu, P. Luo, W. Chen, M. Zheng, J. Hu, K.-Q. Zhang, Z.-S. Wang, L.-S. Liao and M.-P. Zhuo, *Sci. Adv.*, 2023, **9**(50), eadh8917.
8 G. Kwak, Y.-S. Jeong, S.-W. Kim, J.-K. Kim, J. Choi, K. G. Song, H. J. Kim, W. J. Choi, Y. Yang, H.-C. Song, J. M. Baik and H. K. Yu, *Nano Energy*, 2023, **110**, 108336.
9 L. Zhu, T. Ding, M. Gao, C. K. N. Peh and G. W. Ho, *Adv. Energy Mater.*, 2019, **9**, 1900250.
10 J. Sun, T. Fang, H. Wang and S. Wang, *Opt. Continuum*, 2023, **2**, 1638.
11 W. Duan, X. Liu, J. Zhao, Y. Zheng and J. Wu, *ACS Appl. Mater. Interfaces*, 2022, **14**, 48368–48383.
12 M. Lahikainen, H. Zeng and A. Priimagi, *Nat. Commun.*, 2018, **9**, 4148.
13 F. Wu, L. Chen, L. Yue, K. Wang, K. Cheng, J. Chen, X. Luo and T. Zhang, *ACS Appl. Mater. Interfaces*, 2019, **11**, 21408–21416.
14 L. Yue, H. Li, Q. Sun, X. Luo, F. Wu and X. Zhu, *Materials*, 2022, **15**(2), 802.
15 N. M. P. Gosztola, D. Svec, W. Lukas and A. S. Wasielewski, *J. Phys. Chem. A*, 2000, **104**, 6545–6551.
16 M. R. Ajayakumar and P. Mukhopadhyay, *Chem. Commun.*, 2009, 3702–3704, DOI: **10.1039/b903097b**.
17 S. K. Jung, J. H. Heo, D. W. Lee, S. H. Lee, S. C. Lee, W. Yoon, H. Yun, D. Kim, J. H. Kim, S. H. Im and O. P. Kwon, *ChemSusChem*, 2019, **12**, 224–230.
18 J. Qin, F. Lin, D. Hubble, Y. Wang, Y. Li, I. A. Murphy, S.-H. Jang, J. Yang and A. K. Y. Jen, *J. Mater. Chem. A*, 2019, **7**, 6773–6783.
19 J. Shukla, M. R. Ajayakumar and P. Mukhopadhyay, *Org. Lett.*, 2018, **20**, 7864–7868.
20 S. K. Keshri, S. Kumar, K. Mandal and P. Mukhopadhyay, *Chemistry*, 2017, **23**, 11802–11809.
21 R. I. Randle, L. Cavalcanti, S. Sproules and E. R. Draper, *Mater. Adv.*, 2022, **3**, 3326–3331.
22 L. Thomson, R. E. Ginesi, D. D. Osborne, E. R. Draper and D. J. Adams, *Chemistry*, 2023, e202300663, DOI: **10.1002/chem.202300663**.
23 L. Gonzalez, C. Liu, B. Dietrich, H. Su, S. Sproules, H. Cui, D. Honecker, D. J. Adams and E. R. Draper, *Commun. Chem.*, 2018, **1**, 77.
24 R. I. Randle, R. E. Ginesi, O. Matsarskaia, R. Schweins and E. R. Draper, *Macromol. Rapid Commun.*, 2022, e2200709, DOI: **10.1002/marc.202200709**.